www.czasopisma.pan.pl PAN POLSKA AKADEMIA NAUK www.journals.pan.pl

PAN ARCHIVES OF ACOUSTICS
Vol. **45**, No. 4, pp. 663–679 (2020)
DOI: 10.24425/aoa.2020.135254

Research Paper

Radiation Impedance for Square Piston Sources on Infinite Circular Cylindrical Baffles

John L. VALACAS

65 Ag. Varvaras St., Athens,19004 Greece
e-mail: jvalacas@ieee.org

(*received May 31, 2020; accepted July 31, 2020*)

The evaluation of complex radiation impedance for a square piston source on an infinite circular-cylindrical baffle is associated to the Greenspon-Sherman formulation for which novel evaluation methods are proposed. Unlike existing methods results are produced in a very wide range of frequencies and source semi-angles with controllable precision. For this reason closed-form expressions are used to describe the truncation errors of all integrals and infinite sums involved. Impedance values of increased accuracy are also provided in tabulated form for engineering use and a new radiation mass-load model is derived for low-frequencies.

Keywords: cylindrical baffle; radiation impedance; radiation mass-load; piston source.

1. Introduction

The notion of the piston source is fundamental in theoretical Acoustics both in free- and enclosed-space wave propagation. Pressure field and self- or mutual acoustic impedance for piston sources mounted on planar, spherical, cylindrical and spheroidal baffles, play a key-role in textbooks although the realisation of a source vibrating with a uniform velocity profile is not feasible at high frequencies. For rectangular piston sources mounted on infinite planar baffles, several research papers have addressed the evaluation of acoustic impedance with quite different results in terms of precision and (frequency) range of applicability (Swenson, Johnson, 1952; Arase, 1964; Stepanishen, 1977; Levine, 1983; Bank, Wright, 1990; Lee, Seo, 1996; Mellow, Kärkkäinen, 2016). In addition, tabulated impedance values provided by Burnett and Soroka (1972) have become available.

For a cylindrical baffle of radius a (in m), with geometry similar to that of Fig. 1, self- and mutual-radiation impedances have been investigated and their mathematical framework has been established by Greenspon and Sherman (1964). In this framework the evaluation of radiation load is based on a set of three integrals for which no analytic solutions have yet been given. However for this formulation only one numerical evaluation scheme has been proposed by Kim *et al.* (2004), with limited frequency range, source dimensions and accuracy. There has not been any other contribution of extended frequency range and/or source dimensions.

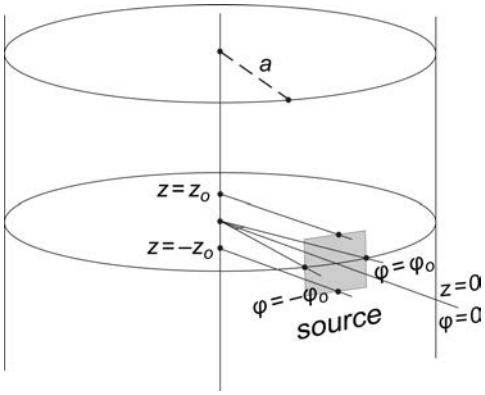

Fig. 1. A rigid square source is mounted on the surface of an infinite cylindrical baffle. It has an angular span $2\varphi_o$, a vertical side $2z_o$ ($z_o = a\varphi_o$) and is located at $z = 0$, $\varphi_o = 0$, $r = a$. φ_o is usually called the source's semi-angle. It is vibrating with a uniform normal vibration velocity.

In the next sections, the original Greenspon-Sherman integrals are briefly presented and novel numerical evaluation methods are described in detail for a wide range of conventional (dimensionless) frequency values ka (where k stands for the usual wavenum-

ber, in m^{-1}) and source semi-angles φ_o (in rad). For practical reasons normalised frequency variable $k\sqrt{S}$ (where S stands for the source's emitting area) is adopted. However when the use of frequency ka simplifies expressions it is preferred. Frequency variables and source semi-angle are related as follows:

$$k\sqrt{S} = 2ka\varphi_o. \tag{1}$$

For the first time to our knowledge, results of significant precision are derived for frequencies in the range $k\sqrt{S}\epsilon$ [0.001, 100] and source semi-angles $\varphi_o\epsilon$ [1, 30] degrees. For the lowest value of source semi-angle $\varphi_o = 1°$, this range leads to conventional normalised frequency values as high as $ka = 2865$. For convenience these results have been tabulated (see Supplement at the end of article). They are also compared to the radiation impedance values of square piston sources on infinite planar baffles so that further verification and useful conclusions be obtained. In addition the low frequency behaviour of radiation reactance values is associated to the widely used mass-load equivalent for which a new approximation model is produced for practical use.

2. The Greenspon-Sherman formulation

Radiation load Z_{mr} is a mechanical impedance quantity expressed in mechanical ohms ($N\cdot s\cdot m^{-1}$). For convenience it is normalised against the medium's characteristic impedance ρcS, where ρ is the medium's density and c the propagation speed:

$$nZ_{mr}\left(k\sqrt{S},\varphi_o\right) = \frac{Z_{mr}}{\rho cS} = nR_{mr} - \mathrm{i}\, nX_{mr}, \tag{2}$$

where nR_{mr} stands for the normalised radiation resistance and nX_{mr} for reactance. Imaginary unit i is defined as $i^2 = -1$.

In their original paper, Greenspon and Sherman presented a formulation for mutual impedance between rectangular pistons on the cylinder's surface that simplifies further in the case of self-radiation impedance. In this framework the equation of (normalised) impedance was broken down to a set of three infinite series of integrals; the first one of them determining the radiation resistance and the other two combining to give reactance. Kim *et al.* (2004) elaborated on this set of equations and added the necessary notation which is adopted in this work as much as possible. After some arrangements of parameters $k\sqrt{S}$, ka and φ_o and narrowing the analysis to square sources ($z_o = a\varphi_o$) the normalised resistance is written as an infinite sum whose terms contain definite integrals I_{msre}:

$$\begin{aligned} nR_{mr}\left(k\sqrt{S},\varphi_o\right) &= \frac{32\varphi_0^2}{\pi^3} I_{sre}\left(k\sqrt{S},\varphi_o\right), \\ I_{sre} &= \sum_{m=0}^{\infty} \frac{\mathrm{sinc}^2(m\varphi_o)}{\varepsilon_m} I_{msre}\left(m,k\sqrt{S},\varphi_o\right), \end{aligned} \tag{3}$$

where $\mathrm{sinc}(x)$ stands for the usual $\sin(x)/x$ function and ε_m is 2 for $m = 0$ and 1 for any other m. Integrals I_{msre} are defined as follows:

$$I_{msre} = \int_0^1 \frac{\mathrm{sinc}^2\left(\frac{1}{2}k\sqrt{S}\,\sqrt{1-t^2}\right)}{t\sqrt{1-t^2}\,D_m(kat)}\,\mathrm{d}t, \tag{4}$$

where $D_m(z)$ is an expression of Bessel functions of the first (J_m) and the second kind (Y_m):

$$D_m(z) = \left(J_{m-1}(z) - J_{m+1}(z)\right)^2 + \left(Y_{m-1}(z) - Y_{m+1}(z)\right)^2. \tag{5}$$

In a similar sense reactance is also written as an infinite sum with terms which, this time, are proportional to the difference of two distinct integrals:

$$\begin{aligned} nX_{mr}\left(k\sqrt{S},\varphi_o\right) &= \frac{8\,ka\,\varphi_0^2}{\pi^2}\left[I_{siy}\left(k\sqrt{S},\varphi_o\right)\right. \\ &\quad \left. - I_{six}\left(k\sqrt{S},\varphi_o\right)\right], \end{aligned} \tag{6}$$

$$I_{siy} = \sum_{m=0}^{\infty} \frac{\mathrm{sinc}^2(m\varphi_0)}{\varepsilon_m} I_{msiy}\left(m,k\sqrt{S},\varphi_o\right), \tag{7}$$

$$I_{six} = \sum_{m=0}^{\infty} \frac{\mathrm{sinc}^2(m\varphi_o)}{\varepsilon_m} I_{msix}\left(m,k\sqrt{S},\varphi_o\right).$$

I_{msiy} are definite integrals while I_{msix} are improper:

$$I_{msiy} = \int_0^1 \frac{B_m(kat)}{D_m(kat)} \frac{\mathrm{sinc}^2\left(\frac{1}{2}k\sqrt{S}\,\sqrt{1-t^2}\right)}{\sqrt{1-t^2}}\,\mathrm{d}t, \tag{8}$$

$$\begin{aligned} I_{msix} &= \int_0^{\infty} \frac{\mathrm{sinc}^2\left(\frac{1}{2}k\sqrt{S}\,\sqrt{1+x^2}\right)}{\sqrt{1+x^2}} \\ &\quad \cdot \frac{K_m(kax)}{K_{m-1}(kax) + K_{m+1}(kax)}\,\mathrm{d}x, \end{aligned} \tag{9}$$

where K_m stands for the modified Bessel function of the second kind and B_m is defined as another expression of Bessel functions of the first and second kind:

$$\begin{aligned} B_m(z) &= J_m(z)\left[J_{m-1}(z) - J_{m+1}(z)\right] \\ &\quad + Y_m(z)\left[Y_{m-1}(z) - Y_{m+1}(z)\right]. \end{aligned} \tag{10}$$

In their integration method, Kim *et al.* (2004) presented results in the frequency range $ka < 51$ and for source semi-angles $\varphi_o < \pi/18$. They regarded orders up to $m = 50$ as sufficient for the sums of Eqs (3) and (7) to converge. They also stopped integration of variable x in I_{msix} at $x = 15$ for an acceptable truncation error to be introduced. In all three integrals they used a variable integration step in order to handle integrand variations in the ranges $t\epsilon$ [0, 1) and $x\epsilon$ [0, 15]. As a result the computation error was estimated to be 0.5% for nR_{mr} and 0.1% for nX_{mr}. The contribution of the singularity point $t = 1$ to definite integrals I_{msre} and I_{msiy} was not considered. In both cases integration was carried up to a t value of 0.9999.

3. The case of I_{msiy} integrals

As already mentioned these are definite integrals in the finite integration range $t\epsilon$ [0, 1]. Their integrand has an obvious singularity at $t = 1$ as per Eq. (8). A change of integration variable ($x = \sqrt{1-t^2}$) leads to a more convenient definition:

$$I_{msiyb}(m,ka,\varphi_o) = ka \int_0^1 F_m\left(ka\sqrt{1-x^2}\right) \cdot \mathrm{sinc}^2(ka\,\varphi_o\,x)\,\mathrm{d}x, \tag{11}$$

where

$$F_m(y) = \frac{B_m(y)}{y\,D_m(y)}. \tag{12}$$

Using ordinary properties of Bessel functions like Eq. (10.6.1) and their series expansions around $y = 0$, like Eqs (10.7.3), (10.8.1) and (10.8.2) in NIST handbook of mathematical functions (Olver *et al.*, 2010), it can be shown that for all orders m above zero $F_m(y)$ tends to $-1/(2m)$ as y tends to 0 (or x tends to 1) and therefore is not singular. In the case of zero-eth order $F_o(y)$, for y tending to zero, we have a logarithmic singularity:

$$\lim_{y\to 0} F_o(y) = \lim_{y\to 0} \frac{1}{2}\left(\ln\left(\frac{y}{2}\right) + \gamma\right) = -\infty, \tag{13}$$

where $\gamma = 0.57721566$ stands for the Euler constant.

However, the major problem is that typical math software fails to compute Bessel functions of the second kind inside F_m, whenever the argument becomes much smaller than the order. To overcome this we note that for small argument values $F_m(y)$ simplifies to:

$$\lim_{y\to 0} F_m(y) = \lim_{y\to 0} \frac{Y_m(y)}{2yY'_m(y)}. \tag{14}$$

Ratio Y_m/Y'_m can be evaluated with a controllable precision for $y < m$ and $m \neq 0$, by Debye expansions as per Eqs (10.19.3) and (10.19.4) in the NIST handbook. Using the polynomials U_k and V_k mentioned in the same reference, a computationally stable estimate for $F_m(y)$ can be obtained ($m \neq 0$):

$$\{F_m(y)\}_{est} = -\frac{1}{2m}\,u\,\frac{\sum_{k=0}^{3}(-1)^k\,\frac{U_k(u)}{m^k}}{\sum_{k=0}^{3}(-1)^k\,\frac{V_k(u)}{m^k}}, \tag{15}$$

$$u = \frac{1}{\sqrt{1-\left(\frac{y}{m}\right)^2}}.$$

The error of this estimate-function drops as argument y decreases towards zero. For every order m and desired error level a critical argument value y_{cr} can be found, below which the estimate-function can safely be used for error-free computation. In this work the maximum acceptable error level was set to 10^{-7} and critical argument values were computed for orders $m = 1$ to $m = 3155$. With frequency $k\sqrt{S}$ no bigger than 100 and $\varphi_o$not less than one degree, ka and thence argument y, is not expected to exceed a value of 3000. Debye expansion proved capable of providing the required precision of 10^{-7} for y-argument values up to 3000 ($y_{cr} = 3000$) for all orders higher than 3155. Figure 2 illustrates a family of several F_m curves as a function of integration variable x.

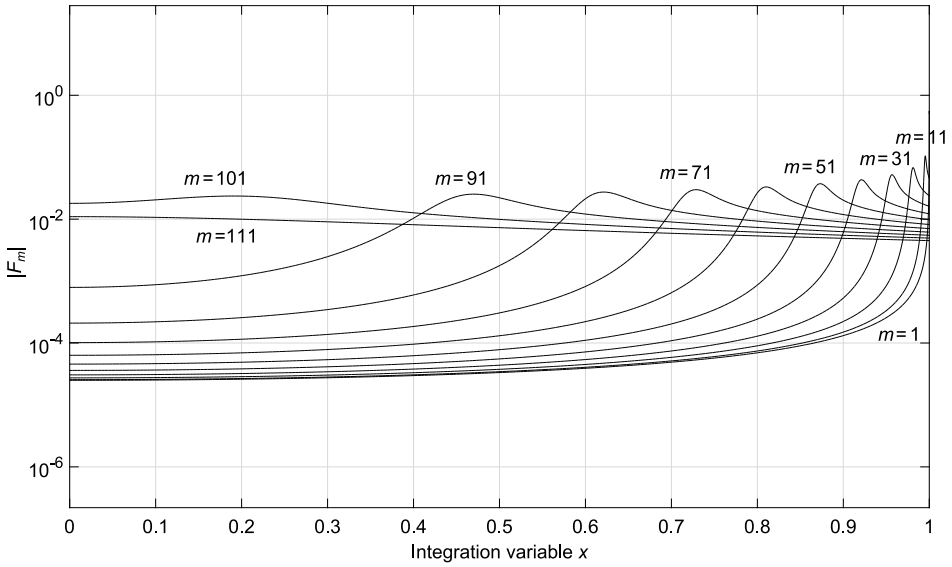

Fig. 2. Plot of a family of F_m curves (absolute values) as a function of integration variable x. Frequency is relatively high ($ka = 100$). Curves exhibit a peak which is close to $x = 1$ for low orders and moves towards $x = 0$ for higher orders m. When either frequency ka is below one or order m exceeds ka value, no peak is present. At $x = 1$ all curves reach the $-1/(2m)$ value.

4. I_{msiy} integration schemes

4.1. Non-singular integrand orders ($m \neq 0$)

The presence of sinc squared factor within the integrand function introduces a number of null points (at $k\sqrt{S}\,x/2$ equal to integer multiples of π) depending on frequency $k\sqrt{S}$. This number will not exceed 15 and may well be zero at low frequencies (see Fig. 3). To ensure a successful evaluation of I_{msiy} integrals, integration range is segmented around these null-points (if any) and Romberg's method is applied to each segment.

4.2. Singular integrand for $m = 0$

To overcome the singularity of the first factor of integrand function, $F_o(y)$, at $x = 1$ ($y = 0$), integration is split into two parts:

$$I_{osiy}\,(ka, \varphi_o) = \int_0^{1-\partial x} + \int_{1-\partial x}^{1} = I_{osiya} + I_{osiyb}, \tag{16}$$

where the first part can be numerically evaluated while the second one can be addressed analytically. ∂x is a small value which must roughly meet three conditions:

- Simple investigation proves that argument y of F_o will go down to a small value ∂y close to zero for which we have $\partial y = ka\sqrt{2\partial x}$. The value of ∂y must allow for a successful evaluation of F_o by typical math software:

$$F_o(y) = \frac{-\left(J_o(y)J_1(y) + Y_o(y)Y_1(y)\right)}{2y\left(J_1(y)^2 + Y_1(y)^2\right)}. \tag{17}$$

  It was found that for this purpose ∂y should not be smaller than 10^{-20}.
- On the other hand, ∂y must be small enough to allow $F_o(y)$ to be approximated by the expression in Eq. (13), in the range 0 to ∂y with a high level of precision. In order to have a worst-case relative error of 10^{-6} at $y = \partial y$, the value of ∂y must not exceed $5 \cdot 10^{-4}$.
- Finally ∂x, being the span of the integration range in I_{osiyb}, must be small enough to allow for the swing of sinc squared factor to be modelled by a simple first-order Taylor expansion or, even better, be considered constant.

All conditions can be met by selecting ∂x to have a fixed value of 10^{-14}, leading to a variable value for ∂y: $1.41 \cdot 10^{-10}$ at $ka = 0.001$ and $4.23 \cdot 10^{-4}$ at $ka = 3000$. Sinc squared factor proves to remain practically unchanged throughout this narrow integration range. The analytic expression for I_{osiyb} becomes:

$$\begin{aligned} I_{osiyb}\,(ka, \varphi_o) &= \frac{ka}{2}\int_{1-\partial x}^{1}\left(\ln\left(\frac{ka\sqrt{1-x^2}}{2}\right)+\gamma\right) \\ &\quad \cdot \operatorname{sinc}^2(ka\varphi_o x)\,\mathrm{d}x = \frac{ka}{2}\operatorname{sinc}^2(ka\varphi_o) \\ &\quad \cdot \int_{1-\partial x}^{1}\left(\ln\left(\frac{ka\sqrt{1-x^2}}{2}\right)+\gamma\right)\mathrm{d}x \\ &= \frac{ka}{2}\operatorname{sinc}^2(ka\varphi_o)\left[\left(\ln\left(\frac{ka}{2}\right)+\gamma\right)\partial x\right. \\ &\quad + \frac{1}{2}\Big(2\ln(2) - (2-\partial x)\ln(2-\partial x) \\ &\quad \left. + \partial x\,\ln(\partial x) - 2\partial x\Big)\right]. \end{aligned} \tag{18}$$

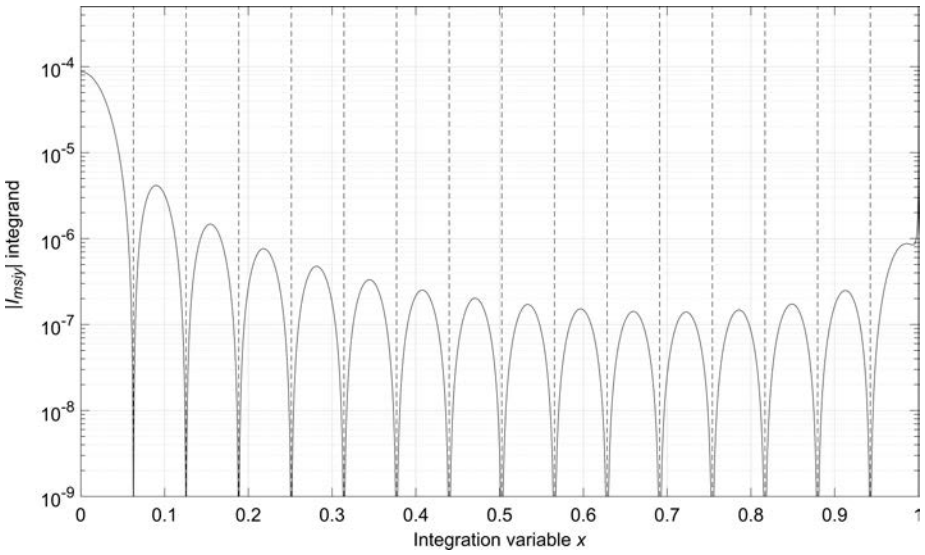

Fig. 3. Plot of absolute value of I_{msiy} Integrand of order $m = 1$ at a frequency of $k\sqrt{S} = 100$ and source semi-angle $\varphi_o = 1$ degree, as a function of integration variable x. Null points due to sinc squared factor lead to segmentation of the integration range for a successful application of Romberg's method.

For the numerical evaluation of I_{osiya}, the segmentation based on sinc squared null-points which was suggested in Subsec. 4.1, is also adopted here along with Romberg's rule. However it must be taken into account that convergence is significantly accelerated by the introduction of additional break-points (and therefore segments) very close to one. Three such points were added close to the right-hand side of the integration range: $1–10^{-3}$, $1–10^{-6}$, $1–10^{-10}$.

At all frequencies and source semi-angles I_{osiyb} values were found several orders of magnitude smaller than the respective I_{osiya} values.

5. I_{siy} summation process

Before addressing the summation process in I_{siy}'s definition in Eq. (7) useful conclusions can be produced by close inspection of I_{msiy} (negative) values' sequences. Figure 4 depicts the decaying nature of these sequences both at low and high frequencies.

At high frequencies a peak is formed at an order m_p approximately equal to frequency parameter ka:

$$m_p \approx \lceil ka \rceil , \tag{19}$$

where $\lceil x \rceil$ is the usual function returning the smallest integer greater than or equal to x. At frequencies close to zero the $|I_{msiy}|$ sequences start to decay just above their first order, i.e. $m_p = 1$ (Fig. 4b).

A second aspect of $|I_{msiy}|$ values is that when plotted with log-log axes, they form, above m_p, a log-log convex sequence. The slope of this sequence is more negative than −10 dB/decade but tends to this value asymptotically. As it is discussed in Appendix A, $|I_{msiy}(m)|$ values will decay faster than a sequence

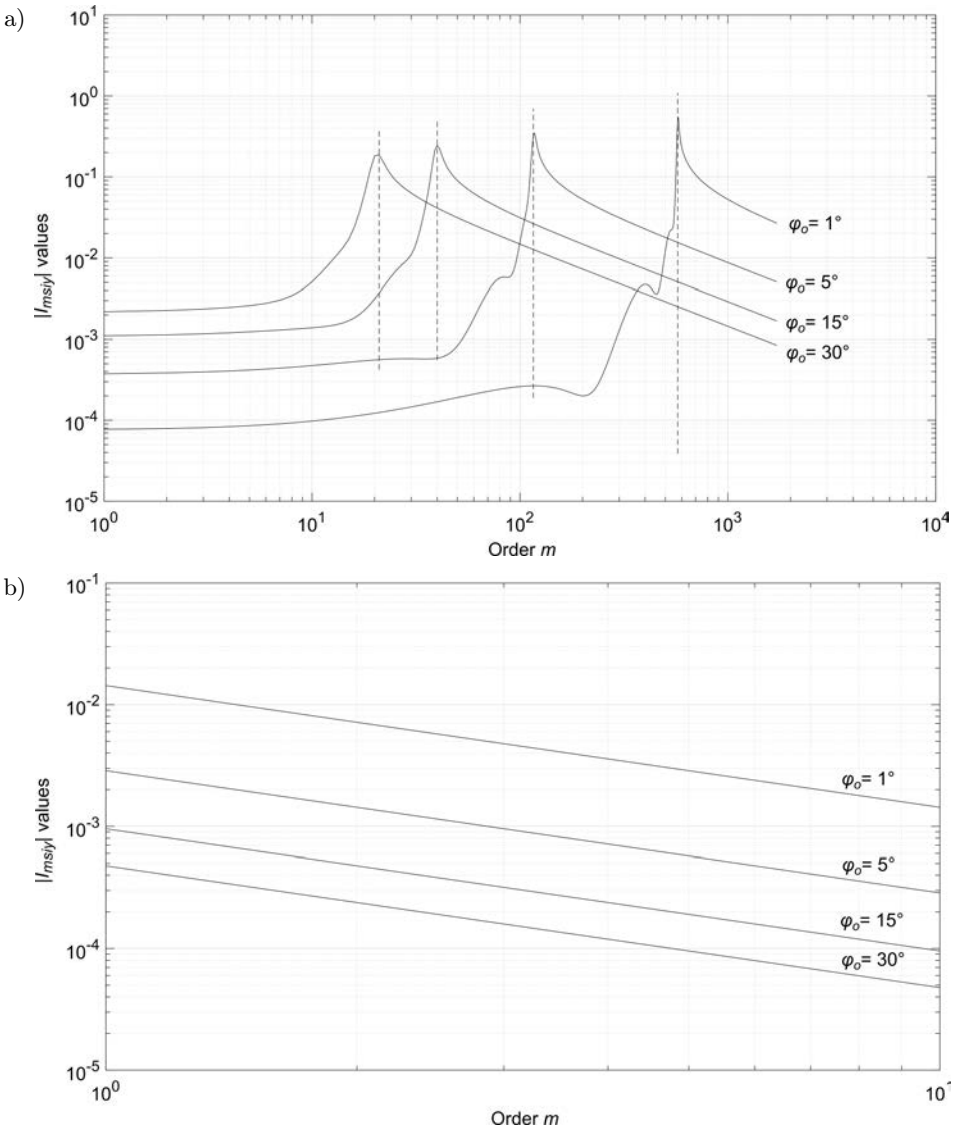

Fig. 4. Graphs of absolute value of $|I_{msiy}|$ integrals as a function of order m for source semi-angles φ_o = 30, 15, 5, and 1 degrees. Above their peak value the decay slope tends asymptotically to −10 dB/decade: a) frequency $k\sqrt{S}$ = 20, b) $k\sqrt{S}$ = 0.001.

proportional to 1/m passing through the point $(m_o, |I_{msiy}(m_o)|)$:

$$\forall\, m_o > m_p,\ \ |I_{msiy}(m \geq m_o)| \leq |I_{msiy}(m_o)| \cdot \frac{m_o}{m}. \quad (20)$$

Having the upper bound described in Eq. (20) allows for the evaluation of the truncation error which will be introduced whenever I_{siy} summation stops at a specific order $m_o - 1$:

$$\begin{aligned}
&\left| \sum_{m=m_o}^{\infty} I_{msiy}(m)\mathrm{sinc}^2(m\varphi_o) \right| \\
&< \sum_{m=m_o}^{\infty} |I_{msiy}(m_o)| \frac{m_o}{m} \frac{\sin^2(m\varphi_o)}{(m\varphi_o)^2} \\
&= |I_{msiy}(m_o)| \frac{m_o}{\varphi_o^2} \sum_{m=m_o}^{\infty} \frac{\sin^2(m\varphi_o)}{m^3} \\
&= |I_{msiy}(m_o)| \frac{m_o}{\varphi_o^2} \left[\frac{1}{2}\mathrm{Li}_3(1) - \frac{1}{4}\mathrm{Li}_3\left(e^{2i\varphi_o}\right) \right. \\
&\quad \left. -\frac{1}{4}\mathrm{Li}_3\left(e^{-2i\varphi_o}\right) - \sum_{m=1}^{m_o-1} \frac{\sin^2(m\varphi_o)}{m^3} \right], \qquad (21)
\end{aligned}$$

where $\mathrm{Li}_3(z)$ stands for the trilogarithm function, a special case of polylogarithm function:

$$\mathrm{Li}_k(z) = \sum_{m=1}^{\infty} \frac{z^m}{m^k}.$$

To put everything together, I_{siy} may proceed unconditionally to sum all orders at least up to m_p and then exit whenever the ratio of the truncation error, per Eq. (21), over the accumulated sum's value, drops below a preselected precision level. In this work this first part of summation was set to include orders up to $70 \cdot m_p$.

6. Investigation of I_{msix} integrals

Integrand function of I_{msix} integrals, given in Eq. (9), can be separated in two factors for further analysis:

$$\begin{aligned}
A_x(ka,\varphi_o,x) &= \frac{\mathrm{sinc}^2\left(\frac{1}{2}k\sqrt{S}\sqrt{1+x^2}\right)}{\sqrt{1+x^2}}, \\
K_{rm}(y) &= \frac{K_m(y)}{K_{m-1}(y) + K_{m+1}(y)} = -\frac{K_m(y)}{2K'_m(y)},
\end{aligned} \quad (22)$$

where y stands for $k\sqrt{S}x/(2\varphi_o)$ or $ka\ x$ and K'_m denotes first-order derivative with respect to argument y.

6.1. The K-function ratio K_{rm}

Although K_m is singular at $y = 0$, the respective ratio K_{rm} is not. Using the limiting forms of Eqs (10.30.2) and (10.31.2) in NIST handbook (Olver *et al.*, 2010) for very small argument, and typical properties of the modified Bessel functions per Watson (1966, p. 79), it can be shown that as y tends to zero K_{rm} tends to $y/(2m)$ for $m > 0$ and to $-(y/2)\ln(y/2)$ for $m = 0$. That is, K_{rm} tends to zero without being singular. On the other hand, when the argument is very large K_{rm} tends to 1/2. In general, $K_m(y)$ has a fast decay so usual mathematical software rounds it to zero when its argument goes beyond a value of 700 approximately and thus reports an error for the ratio K_{rm}. At a frequency of $ka = 100$ this would happen even for relatively small values of integration variable x. Hopefully K_{rm} ratio can be evaluated under some well-stated conditions by other means. For $m = 0$ Yang and Chu (2017, left-hand side of Corollary 3.3 with $p = 1/4$) have provided an upper bound function which can also approximate it as follows:

$$\{K_{r0}(y)\}_{est} = \frac{K_o(y)}{2K_1(y)} \approx \frac{1}{2}\frac{y+\frac{1}{4}}{y+\frac{3}{4}}. \quad (23)$$

A direct comparison of values obtained by typical math software to those given by Eq. (23) proves that for the relative error to be always less than 10^{-5} we must have $y \geq 21$. For all other orders m the Debye expansions per Eqs (10.41.4) and (10.41.6) described in NIST handbook can be used, based on the same polynomials U_k and V_k as in Eq. (15):

$$\begin{aligned}
\{K_{rm}(y)\}_{est} &= \frac{1}{2} \frac{\left(\frac{y}{m}\right)}{\sqrt{1-\left(\frac{y}{m}\right)^2}} \frac{\sum_{k=0}^{3}(-1)^k \frac{U_k(u)}{m^k}}{\sum_{k=0}^{3}(-1)^k \frac{V_k(u)}{m^k}}, \\
u &= \frac{1}{\sqrt{1-\left(\frac{y}{m}\right)^2}}.
\end{aligned} \quad (24)$$

Relative error of Eq. (24) is less than 10^{-7} for all orders $m \geq 25$. Table 1 provides the necessary details.

Table 1. Evaluation rules for K_{rm} ratio.

Order	Range and computation means
$m = 0$	$y < 21$, math software
	$y \geq 21$, Eq. (23)
$1 \leq m < 9$	$y < 10^{-4}$, Eq. (24)
	$10^{-4} \leq y < 40$, math software
	$y \geq 40$, Eq. (24)
$9 \leq m < 25$	$y < 0.10$, Eq. (24)
	$0.10 \leq y < 40$, math software
	$y \geq 40$, Eq. (24)
$m \geq 25$	all y, Eq. (24)

In short, for $m = 0$, K_{rm} starts at $y = 0$ as $-(y/2)\log(y/2)$ and then tends asymptotically to 1/2. For all other orders m it starts as $y/(2m)$ and then tends to 1/2 too.

6.2. The A_x factor

This factor introduces oscillations to I_{msix} integrand with null points nonlinearly spread in integration variable x. It will prove quite useful to know the exact location of either the first f_{np} or the n-th null point n_{np} of this factor and the integrand as a whole:

$$f_{np} = \begin{cases} k\sqrt{S} < 2\pi : \sqrt{\left(\dfrac{2\pi}{k\sqrt{S}}\right)^2 - 1}, \\ k\sqrt{S} \geq 2\pi : \sqrt{\left(\dfrac{\left\lceil \dfrac{2\pi}{k\sqrt{S}} \right\rceil}{\dfrac{2\pi}{k\sqrt{S}}}\right)^2 - 1}, \end{cases} \tag{25}$$

$$n_{np} = \begin{cases} k\sqrt{S} < 2\pi : \sqrt{\left(\dfrac{2n\pi}{k\sqrt{S}}\right)^2 - 1}, \\ k\sqrt{S} \geq 2\pi : \sqrt{\left(\dfrac{\left\lceil \dfrac{2\pi}{k\sqrt{S}} \right\rceil + n - 1}{\dfrac{2\pi}{k\sqrt{S}}}\right)^2 - 1}, \end{cases} \tag{26}$$

where n stands for the integer index of the required n-th null point and $\lceil z \rceil$ is the usual routine that rounds its argument z to the least integer greater than or equal to it.

7. I_{msix} integration scheme

Depending on the relative positions of the 'corner' point after which K_{rm} ratio approaches its asymptotic value and the first null point of A_x, integrand function can take quite different shapes. An example is given in Fig. 5. As in the case of I_{msiy} integrals Romberg's integration rule is adopted. Integration is adjusted to pass through consecutive null points. In this way integration segments adapt to integrand characteristics as frequency and order change.

A loop is used to process initially the first segment up to the first null point $[0,\ f_{np}]$ and then all segments at higher null points. For each loop instance the remaining integral's value i.e. the truncation error, is compared to the accumulated I_{msix} value and when the relative error drops below a pre-selected value the loop stops and integration is concluded. At a point x_o of integration variable x, this remaining value of I_{msix} integral is defined as follows:

$$\{I_{msix}\}_{x_o}^{rem} = \int_{x_o}^{\infty} A_x\,(ka, \varphi_o, x)\ K_{rm}\,(ka\,x)\ \mathrm{d}x. \tag{27}$$

In order to have a safe estimate of this value, upper bound functions are sought for integrand factors A_x and K_{rm}. For A_x the simple property

$$\sin^2(ka\varphi_o\sqrt{1+x^2}) \leq 1$$

is sufficient. For K_{rm} any upper bound that has been proposed in the literature can be used, provided it can lead the integral defined in Eq. (9) to an analytical expression. Such an upper bound for K_{rm}, for $m = 0$,

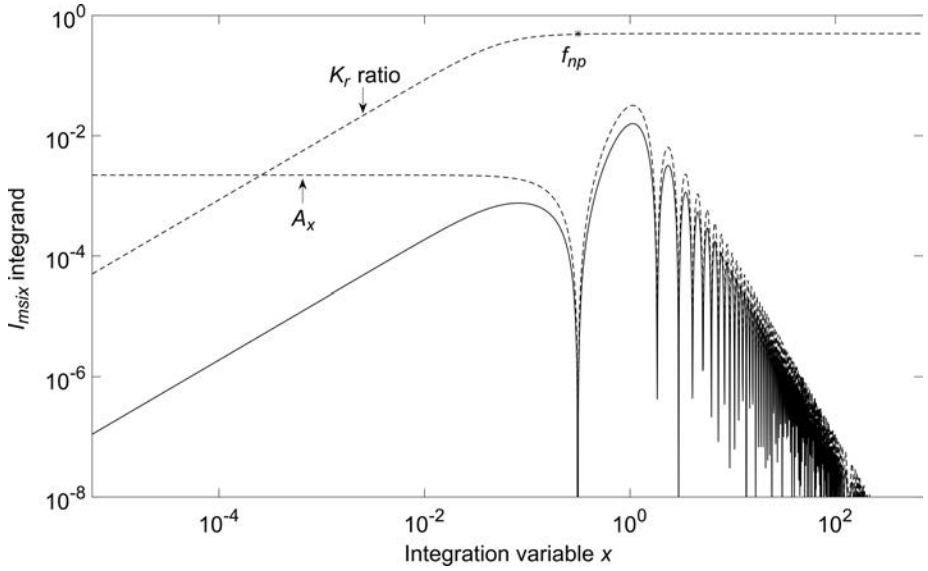

Fig. 5. Graph of I_{msix} integrand function (solid line) for a frequency of $k\sqrt{S} = 6$, source semi-angle $\varphi_o = 1$ degree and order $m = 10$. Dotted lines depict K_r ratio and A_x functions. First null point f_{np} of the latter is also shown for reference.

is Eq. (23) while for $m \neq 0$ the work of Baricz *et al.* (2011, Eq. (5)) can be utilized:

$$K_{rm}(y) < \frac{1}{2}\frac{y}{\sqrt{m^2+y^2}}. \tag{28}$$

As a result, the remaining I_{msix} value can be upper bounded by the following integrals:

$$\{I_{msix}\}_{x_o}^{rem} < \begin{cases} m=0: \dfrac{1}{2}\displaystyle\int_{x_o}^{\infty} \frac{1}{a^*}\frac{x+\frac{1}{4ka}}{x+\frac{3}{4ka}}\,\mathrm{d}x, \\ m\neq 0: \dfrac{1}{2}\displaystyle\int_{x_o}^{\infty} \frac{x\,\mathrm{d}x}{a^*\sqrt{\left(\frac{m}{ka}\right)^2+x^2}}, \end{cases} \tag{29}$$

where

$$a^* = ka^2\varphi_o^2\left(1+x^2\right)^{3/2}.$$

Analytical expressions are obtained and used within the integration process whenever the latter reaches the end of an integration segment:

$$\{I_{msix}\}_{x_o,m=0}^{rem} < \frac{1}{\left(2ka^2\,\varphi_o^2\right)}\left[\frac{\left(3q^2+1\right)\left(\sqrt{1+x_o^2}-x_o\right)+2q}{(9q^2+1)\sqrt{1+x_o^2}}\right.$$

$$\left. +\frac{2q}{(9q^2+1)^{3/2}}\log\left(\frac{\left(\sqrt{9q^2+1}-3q\right)(x_o+3q)}{\sqrt{9q^2+1}\sqrt{1+x_o^2}-3qx_o+1}\right)\right], \tag{30}$$

where $q = 1/(4ka)$ and

$$\{I_{msix}\}_{x_o,m\neq 0}^{rem} < \frac{1}{\left(2ka^2\,\varphi_o^2\right)} \cdot \begin{cases} m=ka: & \dfrac{1}{2\left(1+x_o^2\right)}, \\ m\neq ka: & \dfrac{1}{1-p^2}\left(1-\sqrt{\dfrac{p^2+x_o^2}{1+x_o^2}}\right), \end{cases} \tag{31}$$

where $p = m/ka$.

8. Upper bounds of I_{msix} sequences

When the values of I_{msix} integrals are plotted as a function of order m in a log-log plot, it can be observed that at all frequencies and source semi-angles under consideration, they form decreasing sequences which apart from being log-log concave they also have asymptotes with a slope of −10 dB per decade, i.e. of the form: constant$/m$. Figure 6 illustrates an example which is quite representative of all frequencies.

Using the property of log-log concavity discussed in Appendix B, provides an upper bound for I_{msix} sequences above an order k_o:

$$I_{msix}\left(m \geq k_o\right) \leq I_{msix}(k_o)\cdot\left(\frac{k_o}{m}\right)^{|D|}, \tag{32}$$

where D is the log-log slope of I_{msix} sequence at k_o (per Eq. (50))

$$D = \left(\frac{\log_{10}\left(\frac{I_{msix}(k_o+1)}{I_{msix}(k_o)}\right)}{\log_{10}\left(\frac{k_o+1}{k_o}\right)}\right). \tag{33}$$

9. The I_{six} sum

Generally speaking, the terms of I_{six} sum, defined in Eq. (7), oscillate according to the sinc squared factor and decay at the same time. Their decay is due to the inherent $1/m^2$ decay of the sinc squared factor and the corresponding decay of I_{msix} sequences. The latter was found to tend asymptotically to $1/m$. As a result I_{six} terms are expected to decay as $1/m^3$ at very high orders. As summation advances an effective way to conclude it at a specific order with a controllable truncation error, is to have an estimate of the sum of the remaining infinite terms above that order and thence of the associated relative truncation error.

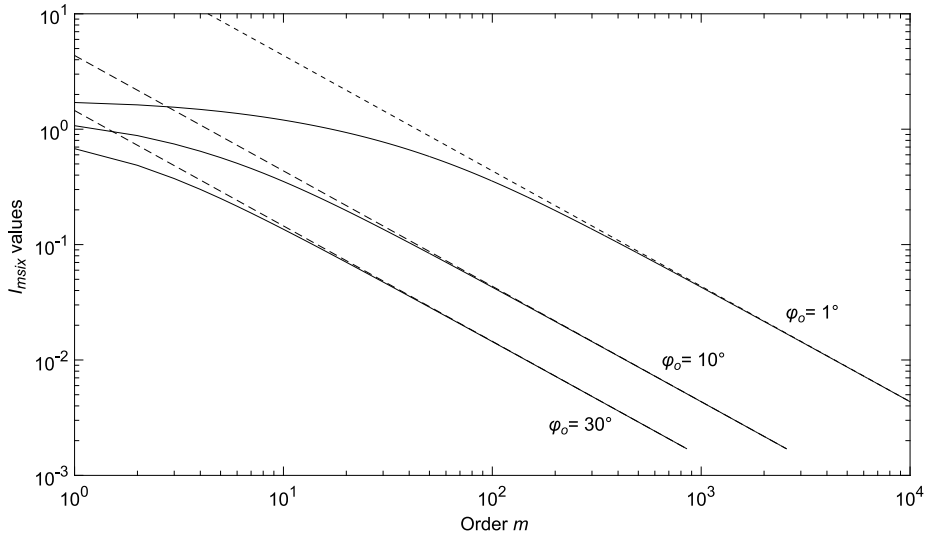

Fig. 6. Plot of I_{msix} sequences for source semi-angles φ_o = 1, 10, and 30 degrees at a frequency $k\sqrt{S} = 0.1$ (solid line). Their asymptotes (dashed) are all lines (powers of m) with slope (exponent) equal to −1.

When the latter drops below a pre-selected value, the whole process can be successfully stopped. In order to apply this idea and after considering several approaches it was decided to work as follows:

- I_{six} sum is carried initially up to an order $k_o - 1$ where $k_o = \left\lceil \frac{450}{2\varphi_o} \right\rceil$ and an upper bound of the sum of the remaining terms is estimated in the following manner:

$$\sum_{m=k_o}^{\infty} I_{msix}(m) \cdot \mathrm{sinc}^2(m\varphi_o) < \sum_{m=k_o}^{\infty} I_{msix}(k_o) \cdot \left(\frac{k_o}{m}\right)^{|D|} \cdot \frac{1}{(m\varphi_o)^2} = I_{msix}(k_o) \cdot \frac{k_o^{|D|}}{\varphi_o^2} \sum_{m=k_o}^{\infty} \frac{1}{m^{2+|D|}}, \quad (34)$$

  where the infinite sum in the right-hand side can be obtained in several ways by means of Zeta, Hurwitz-Zeta or Lerch special functions. For simplicity the use of Zeta function, $\zeta(s)$, was selected (Olver *et al.*, 2010, p. 602):

$$\sum_{m=k_o}^{\infty} \frac{1}{m^{2+|D|}} = \zeta\left(2+|D|\right) - \sum_{m=1}^{m=k_o-1} \frac{1}{m^{2+|D|}}, \quad (35)$$

  where the finite sum $\sum_{m=1}^{m=k_o-1} \frac{1}{m^{2+|D|}}$ is separately computed during the integration process.
- If the ratio of this upper bound (per Eq. (34)) to the current value of I_{six} sum is better (lower) than a target value, the process is concluded, otherwise summation carries on until the relative truncation error drops below the desired value.

10. Radiation reactance

The results of the previous sections on integrals I_{msiy} and I_{msix} along with the associated sums in Eq. (7) produce the radiation reactance nX_{mr} which is a function of frequency $k\sqrt{S}$ and source semi-angle φ_o.

Two major conclusions can be drawn:

- In the case of the square piston on an infinite cylinder with a source semi-angle going down to zero (Figs 7 and 8) the values of normalised reactance tend to the respective values of a square (rectangular) piston on an infinite plane.
- Since low-frequency reactance exhibits a linear dependence on frequency, a mass-load equivalent that the medium presents to the source can be defined as per Beranek (1996, Chap. 5). This mass decreases with increasing semi-angle.

11. Radiation reactance as a mass load

In the field of transducer technology whenever a mechanical reactance is linearly dependent on frequency an equivalent mass load can be defined and used. For piston sources mounted on baffles of infinite extent the quotient of radiation reactance X_{mr} to cyclic frequency ω in the low frequency range where linearity is dominant, defines a mass load M_{mr} in kgr, acting on that side of the vibrating source diaphragm where the medium of propagation is located. A nor-

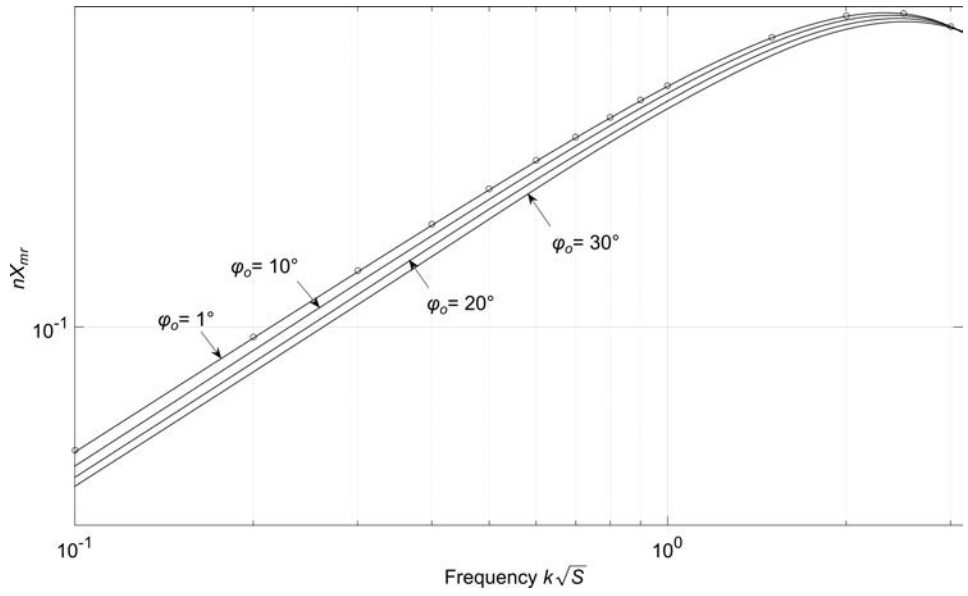

Fig. 7. Comparative graph of the radiation reactance of a square piston on an infinite cylinder (solid lines) and a square piston on an infinite plane as per Burnett and Soroka (1972) (circular marks). Results are given for four source semi-angles.

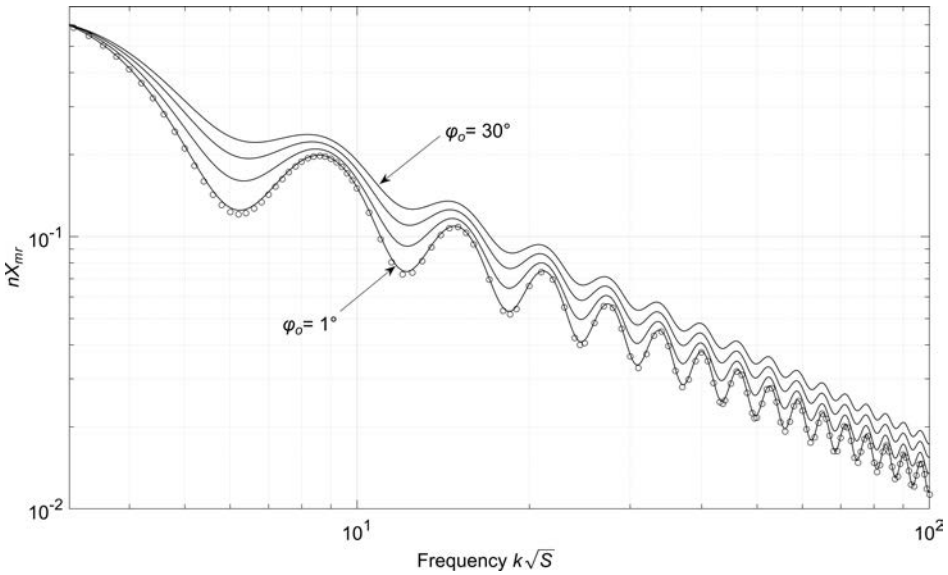

Fig. 8. Graph of $nX_{\mathbf{mr}}$ in the high frequency range for source semi-angles φ_o = 1, 10, 20, and 30 degrees (solid lines). Circle marks indicate the respective reactance for a square piston source mounted on an infinite planar baffle as per Burnett and Soroka (1972).

malised version of mechanical mass load can be related to normalised reactance as follows:

$$nM_{mr} = \frac{M_{mr}}{\rho S^{3/2}} = \frac{X_{mr}}{\omega\rho S^{3/2}} = \frac{nX_{mr}\,\rho cS}{\omega\rho S^{3/2}} = \frac{nX_{mr}}{k\sqrt{S}}, \quad (36)$$

nX_{mr} results in the very low frequency range were tested for linearity and found to satisfy a model of the form $(k\sqrt{S})^q$ with exponent q ranging from 1.000013 at φ_o = 1 degree to 1.0000000006 for φ_o = 30 degrees at lowest frequency $k\sqrt{S}$ = 0.001.

Resulting mass load values are presented in Fig. 9. For convenience a simple polynomial model has also been used to fit these data values and provide an estimate of mass load as a function of source semi-angle φ_o (at $k\sqrt{S}$ = 0.001):

$$nM_{mr} = 0.471 - 0.34\,\varphi_o + 0.72\,\varphi_o^2 - 1.20\,\varphi_o^3 + 0.82\,\varphi_o^4. \quad (37)$$

Obviously this model must not be used for source semi-angles outside the range 1 to 30 degrees. For comparison it is noted that after rearranging the mechanical mass equivalent M_{m1} reported by Beranek (1996, Eq. (5.10)), nM_{mr} for a circular piston on an infinite planar baffle has a value of $8/(3\pi^{3/2})$ = 0.4789.

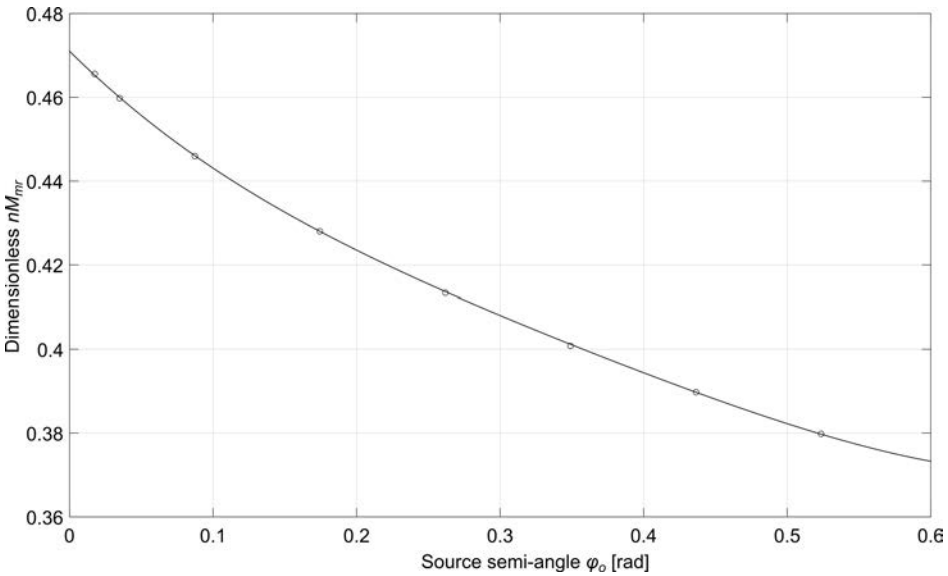

Fig. 9. Values of mass-load nM_{mr} for source semi-angles φ_o = 1, 2, 5, 10, 15, 20, 25, and 30 degrees (circle marks) at $k\sqrt{S}$ = 0.001. Solid line describes estimate model based on Eq. (37).

12. Evaluation of I_{msre} integrals

12.1. Integrand's behaviour

To overcome the singularity of the integrand outlined in Eq. (4) at the rightmost point of the integration range ($t = 1$), a change of integration variable is adopted. Setting $y = \sqrt{1-t^2}$, I_{msre} integral becomes:

$$I_{msre} = \int_0^1 \frac{\operatorname{sinc}^2\left(\frac{1}{2}k\sqrt{S}\,y\right)}{(1-y^2)} \frac{1}{D_m\left(ka\sqrt{1-y^2}\right)}\,\mathrm{d}y = \int_0^1 \operatorname{sinc}^2\left(\frac{1}{2}k\sqrt{S}\,y\right) C_m(ka,y)\,\mathrm{d}y, \quad (38)$$

where C_m function is defined as follows:

$$C_m(ka,y) = \frac{1}{(1-y^2)\,D_m\left(ka\sqrt{1-y^2}\right)}. \quad (39)$$

Using typical power series for the leading terms of $J'_m(z)$ and $Y'_m(z)$ (Olver *et al.*, 2010, Eqs (10.2.2) and (10.8.1), respectively), it becomes apparent that it is the latter that dominates D_m, as argument z tends to zero (y tends to one). The limiting behaviour of C_m for non-zero order m, can therefore be estimated as follows:

$$\lim_{z\to 0} Y'_m(z) = -\frac{m!}{2\pi}\left(\frac{z}{2}\right)^{-m-1} \Rightarrow \lim_{z\to 0}\frac{1}{D_m(z)} = \left(\frac{\pi}{m!}\right)^2\left(\frac{z}{2}\right)^{2m+2} \Rightarrow \lim_{y\to 1} C_m = 0. \quad (40)$$

The case of $m = 0$ is simpler:

$$\lim_{z\to 0} Y'_0(z) = \lim_{z\to 0} -Y_1(z) \Rightarrow \lim_{z\to 0}\frac{1}{D_0(z)} = \left(\frac{\pi}{2}\right)^2\left(\frac{z}{2}\right)^2 \Rightarrow \lim_{y\to 1} C_m = \left(\frac{\pi}{4}ka\right)^2. \quad (41)$$

Conclusively for $m \neq 0$ C_m decays rapidly as the integration variable approaches unity while for $m = 0$ it gets a finite non-zero value. Other interesting properties of factor C_m for non-zero orders m are the following:

- When frequency $ka = k\sqrt{S}/(2\varphi_o)$ is below unity the decay of C_m starts right after $y = 0$.
- When ka exceeds unity this decay is rapid and starts approximately just after a certain value of integration variable, y_p, which depends on order m and frequency ka:

$$y_p = \begin{cases} m \le \lfloor ka \rfloor: & \sqrt{1-\left(\dfrac{m}{\lfloor ka \rfloor}\right)^2}, \\ m > \lfloor ka \rfloor: & 0. \end{cases} \quad (42)$$

- At high frequency values ka and for orders m lower than the integer part of ka, C_m forms a peak around y_p.
- For orders m higher than the integer part of ka, Eq. (42) reports $y_p = 0$ and C_m decays just after $y = 0$.

Figure 10 outlines a typical case of C_m factor for several orders m.

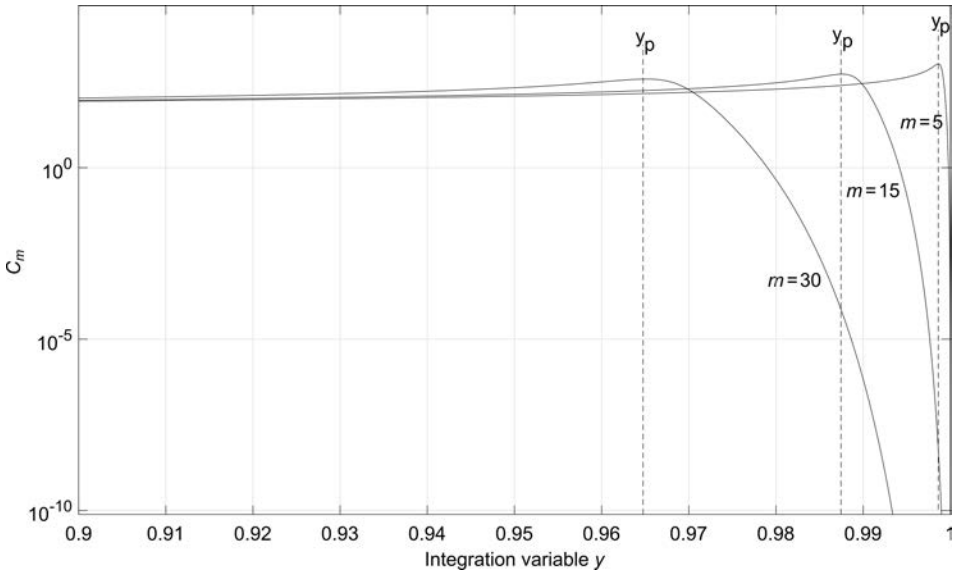

Fig. 10. Graphs of C_m factor for three orders, as a function of integration variable y. Frequency is $k\sqrt{S} = 100$ and source semi-angle $\varphi_o = 30°$. C_m decays just after point $y = y_p$ which generally shifts towards lower values as order m increases.

On the other hand, sinc squared function in Eq. (38) is independent of order m and has the following features:

- It exhibits oscillations only for frequencies $k\sqrt{S} \geq 2\pi$.
- Its first null-point within integration range is located at $y_{fnp} = 2\pi/k\sqrt{S}$.
- Integration range includes $n_{\max}$ null points: $n_{\max} = \lfloor k\sqrt{S}/2\pi \rfloor$.
- Its n-th null-point is at $y_{nnp} = ny_{fnp}$ provided $n \leq n_{\max}$.
- Integration variable can not have a null-point at zero but can definitely have one at unity.

12.2. Integration scheme

It is almost impossible to provide a generalised description of the form that I_{msre} integrand function takes within its finite integration range due to the diversity of its dependencies on frequency $k\sqrt{S}$ (or ka), semi-angle φ_o and order m. For this reason it is more efficient to divide integration range into segments defined by critical points. Such points are the null points of the sinc-squared oscillations (if any) and y_p; the latter possibly being zero for $m > \lfloor ka \rfloor$ or one when $m = 0$. It is very practical to use a vector holding these points prior to the numerical integration process.

Thorough investigation proved that for $m = 0$ this vector is optimum if it takes the generalised form $[0, \text{LHS}_{ynp}, 0.99, \text{RHS}_{ynp}, 1 - \partial, 1]$ where:

- LHS_{ynp} is the set of all the null points below 0.99 and RHS_{ynp} the remaining null points above this value and below $1 - \partial$).
- The injection of point $y = 0.99$ resolves the steep increase of integrand (only for $m = 0$) close to $y = 1$ and is closely related to the required frequency and semi-angle range of values, in this work.
- A very narrow integration segment is defined at the end through the use of a very small quantity ∂. Its purpose is to prevent the computation of integrand (and especially of Eq. (39)) very close to or at $y = 1$ where math software will report errors related to Bessel function of the second kind.

Romberg's integration rule is then applied to all segments except for the last one. Fast convergence and high precision is achieved. Numerical evaluation of the integrand remains successful for a value of ∂ as low as 10^{-15}.

The remaining part of integral (i.e. of the last segment) is evaluated as the area of the trapezoid between points $y = 1 - \partial$ and $y = 1$. Integrand value at $y = 1$ is analytically obtained by Eqs (38) and (41).

For $m \neq 0$ the only general rule is that integrand exhibits a very steep decay close to $y = 1$. This would normally allow for the integration to be ended before reaching the right-hand side integration limit. Unfortunately the location of such a point can not be *a-priori* determined for a given level of truncation error to be maintained. Taking into account that Romberg's rule can not be used for a segment with undetermined limits, a different approach is adopted:

Vector holding the necessary critical points for Romberg's rule to apply, is defined as $[0, \text{LHS}_{ynp}, y_p, \text{RHS}_{ynp}, y_d]$, where:

- The newly introduced y_d denotes a point at which a preselected level of decay of C_m factor has occurred. The introduction of this point extends Romberg's integration close to the end of the overall integration range leaving a relatively narrow range to be separately (and rather slowly) handled.
- Apparently LHS_{ynp} is the set of all possible null points below y_p and RHS_{ynp} the rest of these points above y_p and below y_d.
- Since it is already known that point y_d is definitely in the range $(y_p, 1)$ its evaluation can easily be achieved via an ordinary bisection method targeting a C_m value roughly two orders of magnitude less than the respective value at y_p. Experimentation proved that there is no need for a bigger value of C_m decay.

To ensure both low computation time and high accuracy the remaining integral's part, above y_d, is treated in two phases. In the first one integration advances from y_d towards $y = 1$ in groups of three points via the 1/3 Simpson's rule and at each step an upper bound of the remaining (truncated) integral's value is evaluated and a relative error is associated with it. As soon as the latter drops below a pre-selected value integration is finished and the end-point y_f is marked. In this way points very close to $y = 1$ causing evaluation errors in math software, are avoided. The contribution of this phase to the overall integral is very approximate and therefore should not be stored. In the second phase Romberg's method is applied to segment $[y_d, y_f]$ and the respective contribution is re-evaluated fast and with controllable precision.

To ensure that the end-point y_f always provides the pre-selected level of truncation error without seriously affecting the overall integration time, the first phase employs a very simple, yet overestimated, upper bound of the integral's area to be truncated: the product of the fast-decaying integrand's value (at the point at which the truncation error is sought) and the width of the integration range to be omitted.

13. Sequences of I_{msre} values

Plotting the resulting I_{msre} values for a fixed frequency $k\sqrt{S}$ as a function of order m allows for three major conclusions to be derived (see Fig. 11):

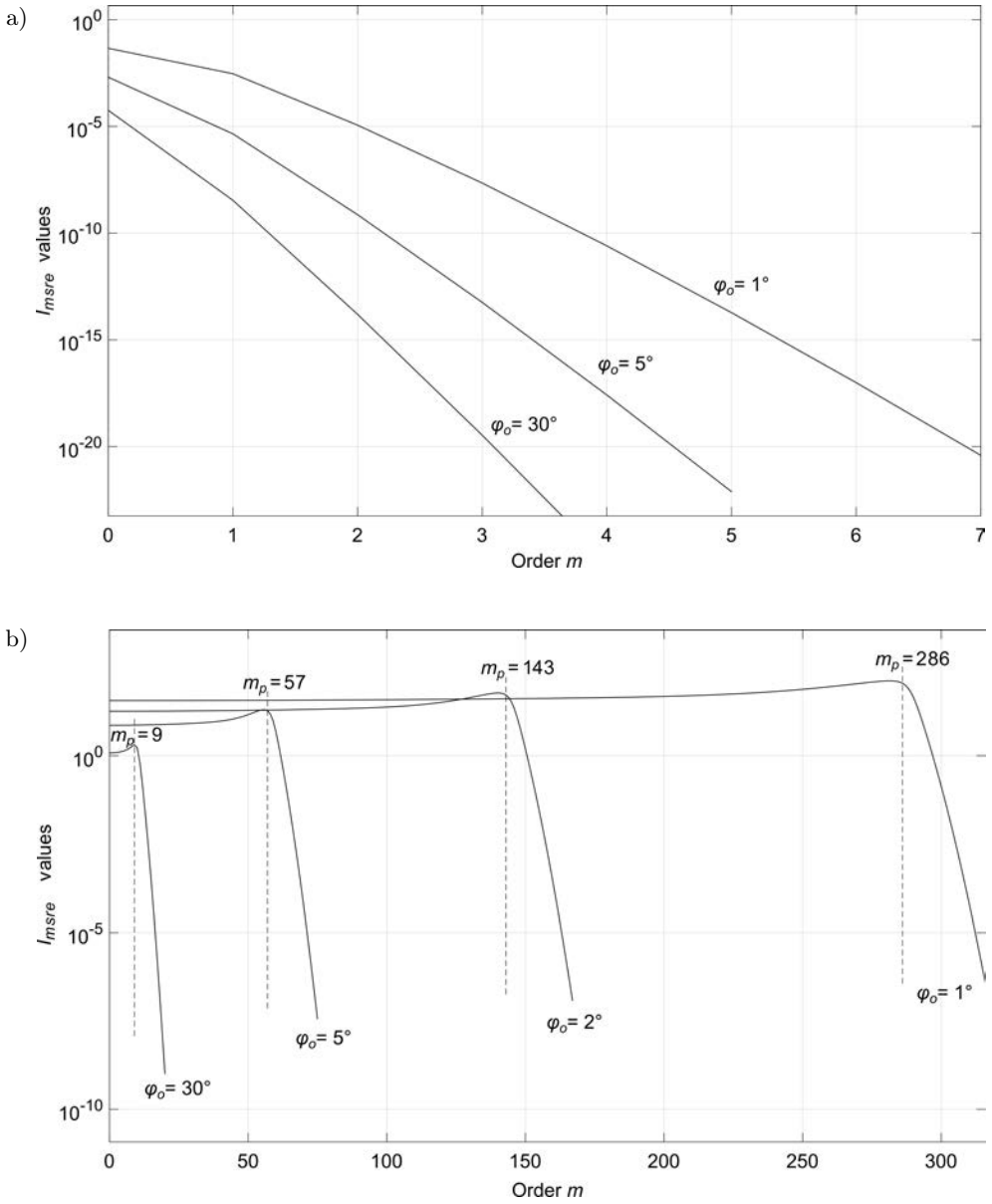

Fig. 11. Plots of I_{msre} values' sequences as a function of order m, for different values of source semi-angle φ_o, at a low and a high frequency value: a) at a frequency of $k\sqrt{S}$ = 0.01 decay occurs just after zero-th order (m_p = 0 for all semi-angles presented), b) $k\sqrt{S}$ = 10.

- I_{msre} values decay faster for larger values of semi-angle φ_o. As a result I_{sre} sum will require much more terms if semi-angle φ_o is lower.
- Roughly speaking I_{msre} values start to decay above order m_p:

$$m_p = \lfloor ka \rfloor . \tag{43}$$

- As frequency $k\sqrt{S}$ (or ka) increases a local peak is formed around m_p. As a rule of thumb I_{sre} sum should definitely include more than the first m_p terms.
- I_{msre} values above m_p form a decreasing log-concave sequence.

14. Summation process for I_{sre}

I_{sre} summation is done per Eq. (3) starting with the first m_p terms (orders) per Eq. (43). As it advances above this order, I_{sre} value is accumulated and the sum of the remaining (infinite) terms (or an upper bound of it) has to be evaluated. The latter represents the truncation error. Summation stops when this error with respect to the accumulated value drops below a pre-selected level.

To derive an expression for the sum of the remaining I_{sre} terms when summation reaches its $k_o - 1$ term we can use Eq. (53) to define an upper bound for I_{msre}

integrals and several quite typical properties of sinc function. A very practical two-fold upper bound for the latter can be expressed according to the value of its argument:

$$\operatorname{sinc}^2(k\varphi_o) < \begin{cases} k < k_\varphi : & 1, \\ k \geq k_\varphi : & \dfrac{1}{(m\varphi_o)^2}, \end{cases} \tag{44}$$

where

$$k_\varphi = \left\lceil \frac{1}{\varphi_o} \right\rceil.$$

As a result we get an expression for the upper bound of the remaining sum which has to break summation depending on the value of order m with respect to k_φ:

$$\sum_{m=k_o}^{\infty} I_{msre}(m) \cdot \operatorname{sinc}^2(m\varphi_o) < \begin{cases} k_o < k_\varphi : & \displaystyle\sum_{m=k_o}^{k_\varphi - 1} I_{msre}(k_o)\, e^{D(m-k_o)} \\ & \quad + \displaystyle\sum_{m=k_\varphi}^{\infty} I_{msre}(k_o)\, e^{D(m-k_o)} \frac{1}{(m\varphi_o)^2}, \\ k_o \geq k_\varphi : & \displaystyle\sum_{m=k_o}^{\infty} I_{msre}(k_o)\, e^{D(m-k_o)} \frac{1}{(m\varphi_o)^2}. \end{cases} \tag{45}$$

Using the Lerch transcendent special function Φ to hold the required infinite sums for the evaluation of Eq. (45) we end up with the following practical expression:

$$\sum_{m=k_o}^{\infty} I_{msre}(m) \cdot \operatorname{sinc}^2(m\varphi_o) < \begin{cases} k_o < k_\varphi : & I_{msre}(k_o) \dfrac{e^{D(k_\varphi - k_o)} - 1}{e^D - 1} \\ & \quad + \dfrac{I_{msre}(k_o)\, e^{D(k_\varphi - k_o)}}{\varphi_o^2} \Phi\left(e^D, 2, k_\varphi\right) \\ k_o \geq k_\varphi : & \dfrac{I_{msre}(k_o)}{\varphi_o^2} \Phi\left(e^D, 2, k_o\right) \end{cases} \tag{46}$$

Lerch function is generally defined as the infinite sum:

$$\Phi(z, n, q) = \sum_{k=0}^{\infty} \frac{z^k}{(k+q)^n}. \tag{47}$$

15. Radiation resistance

Values for the normalised radiation resistance nR_{mr} were obtained for eight source semi-angles (φ_o = 1, 2, 5, 10, 15, 20, 25, and 30°) at a frequency range $k\sqrt{S}$ = 0.001 to 100. In Fig. 12, for convenience, the respective graphs for only four of them are presented along with the radiation resistance of a square piston source mounted on an infinite planar baffle (Burnett, Soroka, 1972).

As frequency increases and radiation condition switches from 4π – to 2π sr, resistance for the case of a tiny source (φ_o = 1°) on a cylinder, tends to almost perfectly match that of a square source on an infinite plane (2π sr radiation).

At very low frequencies (below $k\sqrt{S}$ = 0.015) radiation resistance curves for various source semi-angles become almost identical. As theory predicts all of them are expected to have, at very low frequencies, half the value of the resistance of a (square or equivalent circular) piston source on an infinite planar baffle. For verification purposes, the value of radiation resistance for a circular source on a plane (2π space) was evaluated analytically at $k\sqrt{S}$ = 0.001 (nR_{mr} = $1.591549348 \cdot 10^{-7}$) after Eq. (7.4.31) (Morse, Ingard, 1968). It was found to be twice the value of radiation resistance evaluated by the numerical methods presented in this work for source semi-angle φ_o = 30° ($nR_{mr} = 7.957718476 \cdot 10^{-7}$) for which a 4π space is to be considered since the source dimensions are relatively large compared to cylinder perimeter. Division proves to be correct down to 5 decimal places (2.0000071).

A close investigation of Fig. 12a also shows that radiation resistance switches gradually from the 4π radiation condition to that of 2π-space; the 'transition' occurring at higher frequencies for larger source dimensions (semi-angle).

16. Conclusions

In almost all cases integrands involved in the Greenspon-Sherman formulation were successfully rendered nonsingular except for the zero-eth order of I_{msiy} integral. The latter was addressed analytically by separate integration around its singularity point. However an additional problem related to the required expressions of Bessel functions, was raised. Their computation by typical math software may easily fail either close to integration limits or at very large orders. To overcome this issue Debye expansions were adopted.

On the other hand and in order to control the truncation error and produce results of increased accuracy during integration process, analytical expressions were derived for an upper bound of this error. In a similar way all three (infinite) summation procedures were truncated using analytical upper bounds for the associated error. These bounds were all based on convexity or concavity properties of the respective sequences.

For I_{siy} and I_{sre} sums a lower bound of the number of significant terms was found to be roughly equal to ka. This bound for I_{six} is approximately $225/\varphi_o$. These requirements explain the increased computation error reported by Kim *at al.* (2004). Even for the largest reported semi-angle value of $\pi/18$, I_{six} would require

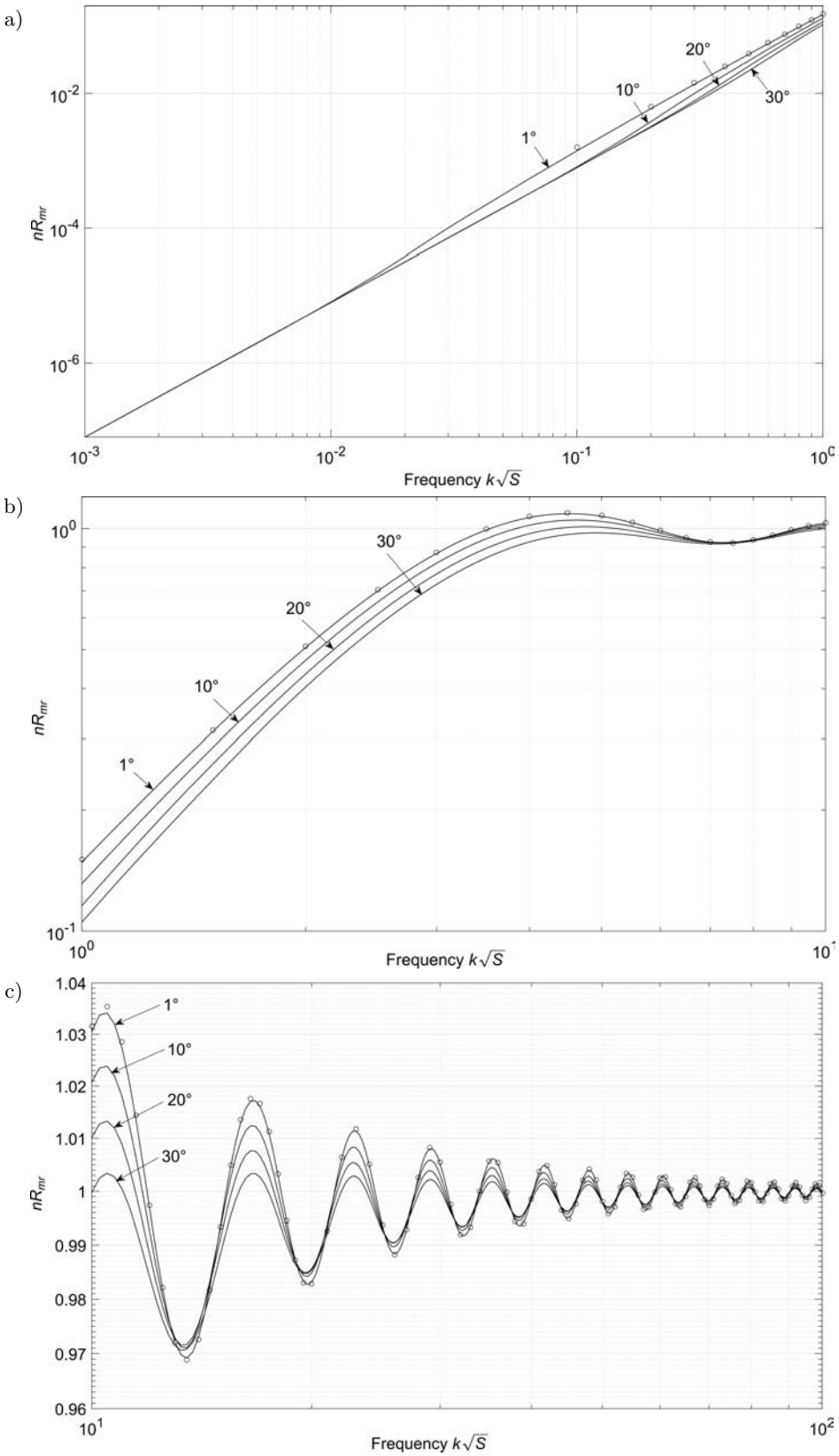

Fig. 12. Normalised radiation resistance nR_{mr} of a square piston on an infinite cylindrical baffle for various source semi-angles φ_o as a function of frequency variable $k\sqrt{S}$. Circle marks correspond to a square piston source mounted on an infinite planar baffle as per Burnett and Soroka (1972): a) very low frequency range; radiation condition changes from 4π to 2π sr at lower frequencies for smaller source semi-angles; b) mid-frequency range; resistance values for a square piston on a planar baffle (circle marks) behaves as an asymptote for sources on a cylinder with semi-angles tending to zero; c) high-frequency range.

more than 1000 terms. The use of orders up to $m = 50$ even for the relatively low frequency range, $ka < 51$, was not sufficient.

Resulting reactance values in the low frequency range were used to derive a model of a radiation mass-load as a function of source semi-angle (Fig. 9). For the first time a clear picture of the decaying oscillations of normalised reactance at high frequencies was also obtained (Fig. 8). As expected when source semi-angle (and thence the source size) tends to zero these values tend to coincide with the respective values of a square piston on a planar baffle as they share a common half-space radiation condition and shape as well.

In the case of radiation resistance results showed that each source semi-angle features its own transition frequency above which the 2π condition is gradually established by the surface of the cylindrical baffle around the source (Fig. 12). As in the case of reactance when source semi-angle approaches zero, resistance values coincide with those of the square piston on a planar baffle.

Impedance values as a function of normalised frequency and source semi-angle were tabulated for convenience (Valacas, 2020). In order for the relative precision of radiation resistance to be always better than 10^{-5}, maximum truncation errors for I_{msre} integral and I_{sre} sum were set to 10^{-7} and 10^{-6} respectively. Romberg's integration routine was adjusted to exit when a relative change of 10^{-7} is achieved. Due to extremely high computation time the target relative error for radiation reactance values was reduced to 10^{-4}. For this purpose the maximum truncation error for I_{msix} integrals was set to 10^{-6} and for the associated I_{six}, I_{siy} sums to 10^{-5}.

In their tabulated form the derived impedance values can be easily related to the design of acoustic emission systems where sources of square (and with a rather good degree of accuracy, of circular) shape are mounted on acoustically-hard cylindrical surfaces as in the case of sonar transducers.

Appendix A

A decreasing log-log convex sequence $b(n)$ of positive terms that above an index n_o has an asymptote of known (log-log) negative slope D, is expected to decay faster than the line $g(n)$ that intersects $b(n)$ at n_o and is parallel to the asymptote:

$$g\left(n \geq n_o\right) = b(n_o)\left(\frac{n_o}{n}\right)^{|D|}. \tag{48}$$

As a result all terms of $b(n)$ have values less than the respective terms of $g(n)$ above n_o:

$$\forall\, n \geq n_o, \qquad b(n) \leq b(n_o)\left(\frac{n_o}{n}\right)^{|D|}. \tag{49}$$

Appendix B

Decreasing log-log concave sequences $b(n)$ (of positive terms) above an index n_o are known to decay faster than the tangent line $g(n)$ that 'touches' $b(n)$ at n_o and has the same slope with $b(n)$ at n_o. In order for sequence $g(n)$ to maintain the linear form in a log-log plot, it has to be proportional to an inverse power of n as per Eq. (48) with D as the negative slope of sequence $b(n)$ at n_o:

$$D = \left(\frac{\log_{10}\left(\frac{b(n_o+1)}{b(n_o)}\right)}{\log_{10}\left(\frac{n_o+1}{n_o}\right)}\right). \tag{50}$$

It can therefore be stated that $g(n)$ serves as an upper bound of $b(n)$ above n_o as per Eq. (49).

Appendix C

In the case of a decreasing sequence $b(n)$ (of positive terms) which above an index n_o exhibits log-concavity we can define its tangent line $g(n)$, at n_o and use it as an upper bound for sequence $b(n)$ above n_o. For sequence $g(n)$ to exhibit the linear form in a log plot and at the same time be tangent to $b(n)$ at n_o, it must be of an exponential type:

$$g(n \geq n_o) = b(n_o)e^{D(n-n_o)}, \tag{51}$$

where D stands for the logarithmic slope of $g(n)$ (and $b(n)$) at n_o:

$$D = \ln\left(\frac{b(n_o+1)}{b(n_o)}\right). \tag{52}$$

Although log-concave sequences and their tangent lines can be described with logarithms of any base, the natural logarithm and its associated base were selected in this work for convenience.

As before it can be asserted that values of $b(n)$ sequence, above n_o, are bounded as follows:

$$b(n \geq n_o) \leq b(n_o)\, e^{D(n-n_o)}. \tag{53}$$

References

1. Arase E.M. (1964), Mutual radiation impedance of square and rectangular pistons in a rigid infinite baffle, *The Journal of Acoustical Society of America*, **36**(8): 1521–1525, doi: 10.1121/1.1919236.
2. Bank G., Wright J.R. (1990), Radiation impedance calculations for a rectangular piston, *Journal of the Audio Engineering Society*, **38**: 350–354.
3. Baricz Á., Ponnusamy S., Vuorinen M. (2011), Functional inequalities for modified Bessel functions, *Expositiones Mathematicae*, **29**(4): 399–414, doi: 10.1016/j.exmath.2011.07.001.
4. Beranek L.L. (1996), *Acoustics*, Acoustical Society of America, Cambridge, MA.

5. Burnett D.S., Soroka W.W. (1972), Tables of rectangular piston radiation impedance functions, with application to sound transmission loss through deep apertures, *The Journal of Acoustical Society of America*, **51**(5B): 1618–1623, doi: 10.1121/1.1913008.
6. Greenspon J.E., Sherman C.H. (1964), Mutual-radiation impedance and nearfield pressure for pistons on a cylinder, *The Journal of Acoustical Society of America*, **36**(1): 149–153, doi: 10.1121/1.1918925.
7. Kim J.S., Kim M.J., Ha K.L., Kim C.D. (2004), Improvement of calculation for radiation impedance of the vibrators with cylindrical baffle, *Japanese Journal of Applied Physics*, **43**(5B): 3188–3192, doi: 10.1143/JJAP.43.3188.
8. Lee J., Seo I. (1996), Radiation impedance computations of a square piston in a rigid infinite baffle, *Journal of Sound and Vibration*, **198**(3): 299–312, doi: 10.1006/jsvi.1996.0571.
9. Levine H. (1983), On the radiation impedance of a rectangular piston, *Journal of Sound and Vibration*, **89**(4): 447–455, doi: 10.1016/0022-460X(83)90346-2.
10. Mellow T., Kärkkäinen L. (2016), Expansions for the radiation impedance of a rectangular piston in an infinite baffle, *The Journal of Acoustical Society of America*, **140**(4): 2867–2875, doi: 10.1121/1.4964632.
11. Morse P.M., Ingard K.U. (1968), *Theoretical Acoustics*, Princeton University Press, Princeton, New Jersey.
12. Olver F.W.J., Lozier D.W., Boisvert R.F., Clark C.W. [Eds], (2010), *NIST Handbook of Mathematical Functions*, NIST & Cambridge University Press.
13. Stepanishen P.R. (1977), The radiation impedance of a rectangular piston, *Journal of Sound and Vibration*, **55**(2): 275–288, doi: 10.1016/0022-460X(77)90599-5.
14. Swenson G.W., Johnson W.E. (1952), Radiation impedance of a rigid square piston in an infinite baffle, *The Journal of Acoustical Society of America*, **24**(1): 84, doi: 10.1121/1.1906856.
15. Valacas J. (2020), *Tabulated values for radiation impedance of a square piston source on a circular cylindrical baffle*, Mendeley Data Repository, http://dx.doi.org/10.17632/rvwffybpdw.3.
16. Watson G.N. (1966), *A Treatise on the theory of Bessel Functions*, 2nd Ed., Cambridge University Press.
17. Yang Z.H., Chu Y.M. (2017), On approximating the modified Bessel function of the second kind, *Journal of Inequalities and Applications*, **1**: 1–8, doi: 10.1186/s13660-017-1317-z.